Stabilized Lithium–Sulfur Batteries by Covalently Binding Sulfur onto the Thiol-Terminated Polymeric Matrices

Xuejun Liu, Na Xu, Tao Qian,* Jie Liu, Xiaowei Shen, and Chenglin Yan*

Despite the low competitive cost and high theoretical capacity of lithium–sulfur battery, its practical application is severely hindered by fast capacity fading and limited capacity retention mainly caused by the polysulfide dissolution problem. Here, this paper reports a new strategy of using thiol-terminated polymeric matrices to prevent polysulfide dissolution, which exhibits an initial capacity of 829.1 mAh g^{-1}, and the exceptionally stable capacity retention of ≈84% at 1 C after 200 cycles, and excellent cycling stability with a low mean decay rate of 0.048% after 600 cycles. Significantly, in situ UV/vis spectroscopy analysis of the electrolyte upon battery cycling is performed to verify the function of preventing polysulfide dissolution by means of strongly anchoring discharge products of lithium sulphides. Moreover, density functional theory calculations reveal that the breakage of the linear sulfur chains results in the less soluble short-chain polysulfides due to the formation of the covalently crosslinked discharge products, which avoids the production of soluble long-chain polysulfide and minimizes the shuttle effect. These results exhibit an alternative for the stabilization of the electrochemical performance of lithium–sulfur batteries.

As one of the most abundant elements in nature, almost 70 million tons of element sulfur is produced annually and the production is believed to grow quickly. However, the increasing expansion of the global sulfur production, coupled with the limited demand, creates a huge surplus of elemental sulfur.[1] Therefore, the development of innovative chemical methods for the direct utilization of sulfur offers an intriguing new direction for recycling the abundant sulfur. The common stable form of sulfur is an eight-member ring (S_8) with an orthorhombic structure. When the solid sulfur is heated to 95 °C, the crystal goes from orthorhombic to monoclinic, then melts at a temperature of 120 °C. Further heating above 160 °C results in equilibrium ring-opening polymerization of S_8 and formation of the linear sulfenyl diradicals.[2] However, it should be pointed out that the linear polymers are thermodynamically unstable and will slowly

revert to cyclooctasulfur when cooled.[3] Hence, the use of free radical copolymerization strategy that incorporates element sulfur into polymeric materials has been explored to modify the properties of element sulfur.[4]

Lithium–sulfur batteries, which exploit reversible conversion reaction of sulfur with lithium ions, could theoretically achieve the energy density several times higher than that of the lithium-ion batteries.[5] Thus, the combination of lithium and sulfur has shown great promise as an alternative option for full electrification of vehicles. Despite the enticing characteristics of lithium–sulfur batteries, several challenges associated with sulfur cathodes still need to be addressed. Besides the low electronic and ionic conductivities of sulfur and polysulfide,[6] lithium–sulfur batteries also suffer from significant volumetric change, ≈80% during charging and discharging cycles.[7] Moreover, the shuttling effect arising from dissolved polysulfide intermediates causes an inevitable loss of sulfur.[8] All of these problems result in limited use of active materials, reduced efficiency as well as poor cycle performance. To resolve these challenges, considerable efforts have been made to encapsulate sulfur within various porous carbon materials and conducting polymers,[9] which not only increase the electrical conductivity but also prevent the loss of the soluble polysulfides. However, it is difficult to avoid the dissolution and migration of the polysulfide species merely by physical adsorption between the nonpolar carbons and the polar polysulfides. Therefore, modifying the carbon host with polar and conductive materials offers an alternative to improve the anchor effect for polysulfides.[10] However, it is still unable to avoid the production and dissolution of polysulfides. To overcome these problems, copolymerization strategies that covalently integrate the sulfur into the polymeric matrices have been adopted to prepare the sulfur-rich polymers for Li–S batteries. For example, Pyun[11] and co-workers described the direct copolymerization of the sulfur with vinylic monomers, exhibiting enhanced battery performance compared to pure sulfur. Using the similar method, Coskun[12] and co-workers prepared a covalent triazine framework, which is proved to be promising as the sulfur cathode material, while the weak conducting characteristics of sulfur-containing polymers still needs to be resolved.

Herein, we developed a new strategy to covalently stabilize the discharge products of lithium–sulfur batteries by covalently binding the sulfur onto the thiol-terminated polymeric

X. Liu, N. Xu, Dr. T. Qian, J. Liu, X. Shen, Prof. C. Yan
College of Physics
Optoelectronics and Energy & Collaborative Innovation Center of Suzhou
Nano Science and Technology and Key Laboratory of Advanced Carbon
Materials and Wearable Energy Technologies of Jiangsu Province
Soochow University
Suzhou 215006, China
E-mail: tqian@suda.edu.cn; c.yan@suda.edu.cn;
chenglinyan.nano@gmail.com

The ORCID identification number(s) for the author(s) of this article can be found under https://doi.org/10.1002/smll.201702104.

ADVANCED
SCIENCE NEWS
www.advancedsciencenews.com

NANO · MICRO
small
www.small-journal.com

matrices. Specifically, thiol-terminated 2-amino-1,3,5-triazaine-4,6-dithiol (ATD) is chosen as a medium to react with graphene oxide (GO) and simultaneously introduce thiol groups, which are covalently bonded onto the surface of graphene nanosheets. The thiol group grafted graphene is used to initiate the radical reaction between thiol groups and diradical polymeric sulfur, forming the interconnected graphene framework. Meanwhile, graphene nanosheets are used as the host to immobilize the sulfur species, benefiting to the electrical conductivity as well as the cycling performance, which could effectively prevent the appearance of soluble long-chain polysulfides. The unique molecular structure makes it an ideal cathode material for Li–S battery, exhibiting excellent capacity retention of 0.048% per cycle for 600 cycles and high capacity compared to sulfur-rich polymers. To understand the evolution process of discharge products during electrochemical reaction, in situ UV/vis spectroscopy is conducted. From the measured set of spectra it can be inferred that short-chain polysulfides are produced as the main discharge products. Further confirmation is shown by quantitative investigation on the cleavage of S—S bonds, as calculated by density functional theory (DFT). The calculations imply that the crosslinked sulfur chains in ATD-functionalized graphene–sulfur (AFG/S) nanocomposites are prone to broke in the middle position, with the lowest dissociation energy of -16.14 kcal mol^{-1} for the S_4—S_5 bond. Further cleavage results in the formation of polysulfides with short-chains. Our study

presents an effective strategy to covalently confine the sulfur onto the graphene for lithium–sulfur batteries and is helpful to explore the electrochemical mechanism involved.

Schematic illustration of the synthesis of AFG/S copolymers is shown in **Figure 1**a. Initially, ATD molecules were covalently linked onto the GO nanosheets through nucleophilic attack to the epoxy carbon and β-carbon of $-$OH.[13] After lyophilization, the as-prepared AFG powders were ground with sulfur, followed by heating the mixture at 160 °C for 10 h in order to ensure the homogeneous distribution of sulfur among the surface of AFG. After that, ring-opening polymerization of elemental sulfur at the thiol surfaces of AFG occurred by further heating to 245 °C, the temperature at which the cyclic S_8 molecules transform to the linear sulfenyl diradicals and crosslinked by the thiol end-group of AFG sheets. The microstructure of AFG is characterized by transmission electron microscope, as shown in Figure 1b. The layered AFG nanosheets with wrinkled structure are clearly observed. The corresponding elemental mappings of C, S, and N presented in Figure 1d–f reveal that thiol groups are homogeneously distributed across graphene surface. To investigate the surface chemical composition of the prepared sample, X-ray photoelectron spectroscopy is employed, as shown in Figure S1 of the Supporting Information. For GO, only C 1s and O 1s signals are detected. After ATD functionalization, three new peaks located at 400.4, 164.5, and 228.2 eV are observed in AFG, corresponding to N 1s,[14]
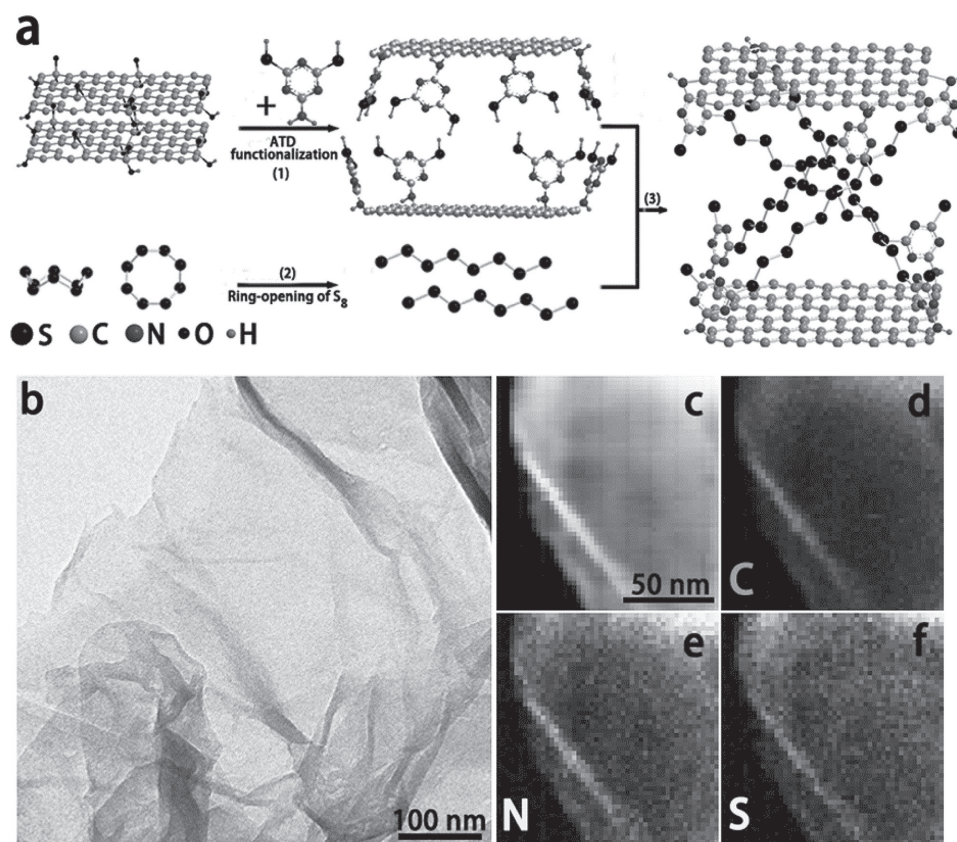

Figure 1. a) Schematic illustration showing the synthetic procedures of AFG/S copolymers. (1) Functionalization of graphene with ATD molecules, (2) ring-opening reaction of S_8, and (3) homogeneous distribution of sulfur followed by the covalently crosslinked sulfur on graphene. b) TEM image of AFG nanocomposites and the corresponding element mapping for d) C, e) N, and f) S.

ADVANCED
SCIENCE NEWS
www.advancedsciencenews.com

NANO · MICRO
small
www.small-journal.com

S 2p, and S 2s.[15] The atomic amount of sulfur and carbon in AFG is measured to be 6.53% and 59.63%. Supposed that all the linear sulfenyl diradicals are covalently bonded on the thiol end-group of graphene sheets, the theoretical content of sulfur is calculated to be 53.8%. In the meantime, AFG shows an obviously increased C/O ratio compared with GO. All these results indicate that ATD functionalization could not only introduce thiol groups to covalently bind the sulfur species, but also enhance the conductivity of the AFG nanosheets by reducing oxygen defects of GO[16] (Figure S2, Supporting Information). For the sample AFG/S copolymers, the subsequent sulfur attachment results in the increased intensity of the peaks assigned to S 2p and S 2s. In the high-resolution S 2p spectra, the peaks appeared at around 163.8 and 165.1 eV can be assigned to S $2p_{3/2}$ and S$2p_{1/2}$.[17] Another two peaks are located at around 162.8 and 163 eV, corresponding to −C−S− bonding.[18] The results demonstrate that sulfur has successfully anchored on AFG by covalent binding. Thermogravimetric analysis was used to determine the overall content of sulfur in AFG/S copolymers. As shown in Figure S3 of the Supporting Information, the total sulfur content in AFG/S is calculated to be about 60%.

The electrochemical properties of the AFG/S copolymers were studied using the copolymers as the cathode, and Li foil as the anode. Controlled cells were fabricated using GO/S as the cathode. **Figure 2**a shows the representative galvanostatic charge–discharge voltage profiles of AFG/S cathode within the voltage window of 1.7–2.7 V, which is consistent with the results shown in the current–voltage curves (Figure S4, Supporting Information). Comparison of the discharge profiles

between the second and the 100th cycles reveals negligible changes in both shape and specific capacity. The cycling performance of AFG/S as well as GO/S was tested at a current density of 1 C, as shown in Figure 2b. The AFG/S delivers an initial discharge capacity of 829.1 mAh g^{-1}. After 100 cycles, a reversible discharge capacity of 704.8 mAh g^{-1} is maintained, representing excellent capacity retention of 94.6% based on the second cycle. Meanwhile, a high efficiency of 99.3% is remained, suggesting that the covalent attachment of sulfur onto the thiol grafted graphene can effectively improve reversible performance. By contrast, an initial capacity of 584 mAh g^{-1} is observed for GO/S cathode. After 100 cycles, the capacity retention of 77.1% is obtained, which is arising from the adsorbing ability of oxygen-containing groups to S. After chemical reduction by hydrazine hydrate, reduced GO (rGO)/S delivers higher capacity of 910.3 mAh g^{-1}. But the oxygen-containing groups on rGO surface are largely removed, leading to the weak interaction between rGO and S. Thus relatively low capacity retention of 40% (100 cycles) is observed for rGO/S (Figure S5, Supporting Information). Figure S6 of the Supporting Information presents the rate performance of AFG/S cathode cycled at various C-rates. The cathode presents the average reversible capacities of 1076, 931, 812, and 665 mAh g^{-1} as the current density increases from 0.2 to 2 C. When the C-rate is switched abruptly from 2 to 1 C, the original capacity is largely recovered, revealing the excellent stability of the cathode materials. Figure 2c illustrates the cycling performance of the AFG/S cathodes at different current densities. After 200 cycles, the cells could still remain relatively high capacity, with excellent capacity retention of 84%, 81%, and 78%, at 1, 1.5, and
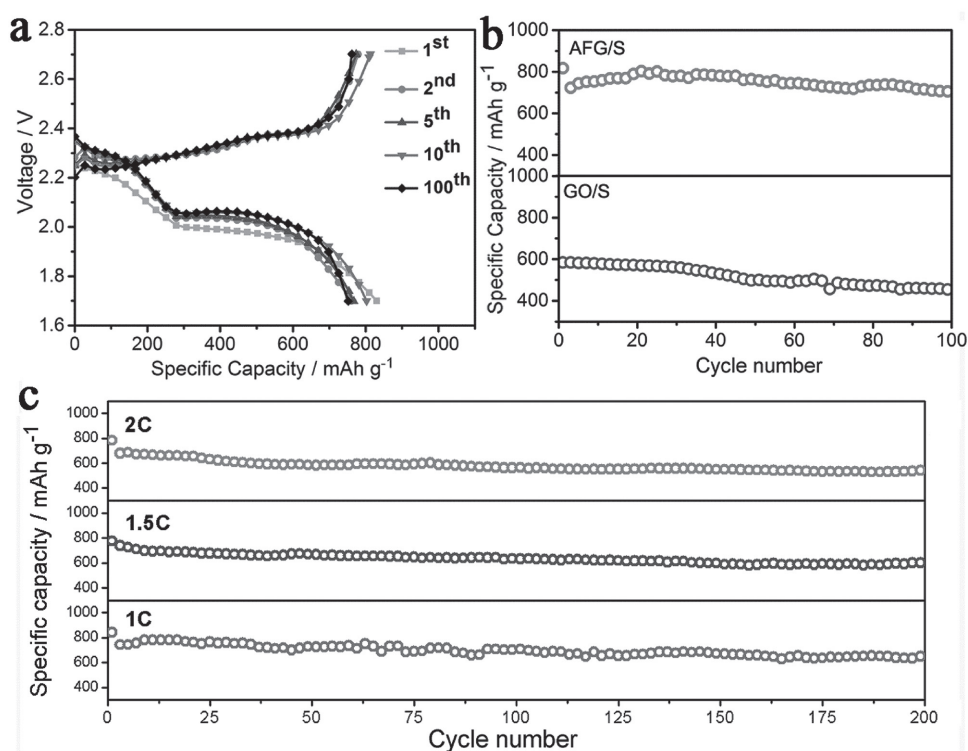

Figure 2. a) Galvanostatic charge–discharge voltage of AFG/S nanocomposites for the 1st, 2nd, 5th, 10th, and 100th cycles. b) Cycling performance of AFG/S copolymers and GO/S composites. (c) The cycling performance of AFG/S copolymers cathode at 1, 1.5, and 2 C for 200 cycles.

2 C, respectively. The long-term cycling performance of AFG/S copolymers was tested at a current density of 1 C. As shown in Figure S7 of the Supporting Information, the cell exhibits an initial capacity of 829.1 mAh g^{-1}. After 600 cycles, the cell exhibits excellent cycling stability with a low mean decay rate of 0.048%. Moreover, the AFG/S cathode exhibits a high specific capacity of 971.5 and 848.7 mAh g^{-1} at 0.2 C when increasing the sulfur loading to 2.1 and 3.2 mg cm^{-2}, respectively, corresponding to areal capacity of 2.04 and 2.72 mAh cm^{-2} (Figure S8, Supporting Information). To further illustrate the excellent capacity retention properties discussed above, in situ visual-electrochemical study was examined in an optically transparent Li–S cell. Representative results are given in Figure S9 of the Supporting Information. The increasingly changed color of electrolyte from colorless to green-yellow is

observed for the rGO/S composites (due to the formed long-chain polysulfides), contrary to the colorless electrolytes for the AFG/S nanocomposites.

In situ UV/vis spectroscopy evaluated at different states during charging and discharging was conducted to better understand the stabilization mechanism of the covalent structure for Li–S batteries,[19] which is based on the perforated negative case with a sealed cover glass for detect of polysulfides (as shown in **Figure 3**a,b). UV/vis spectra for GO/S composites clearly reveal the formation of different types of lithium polysulfide intermediates. As shown in Figure S10c of the Supporting Information, the absorption shifts toward higher wavelengths when the cell is discharged to 2.09 V, during which long-chain polysulfides are formed. Further discharging to 1.69 V results in the movement of absorption
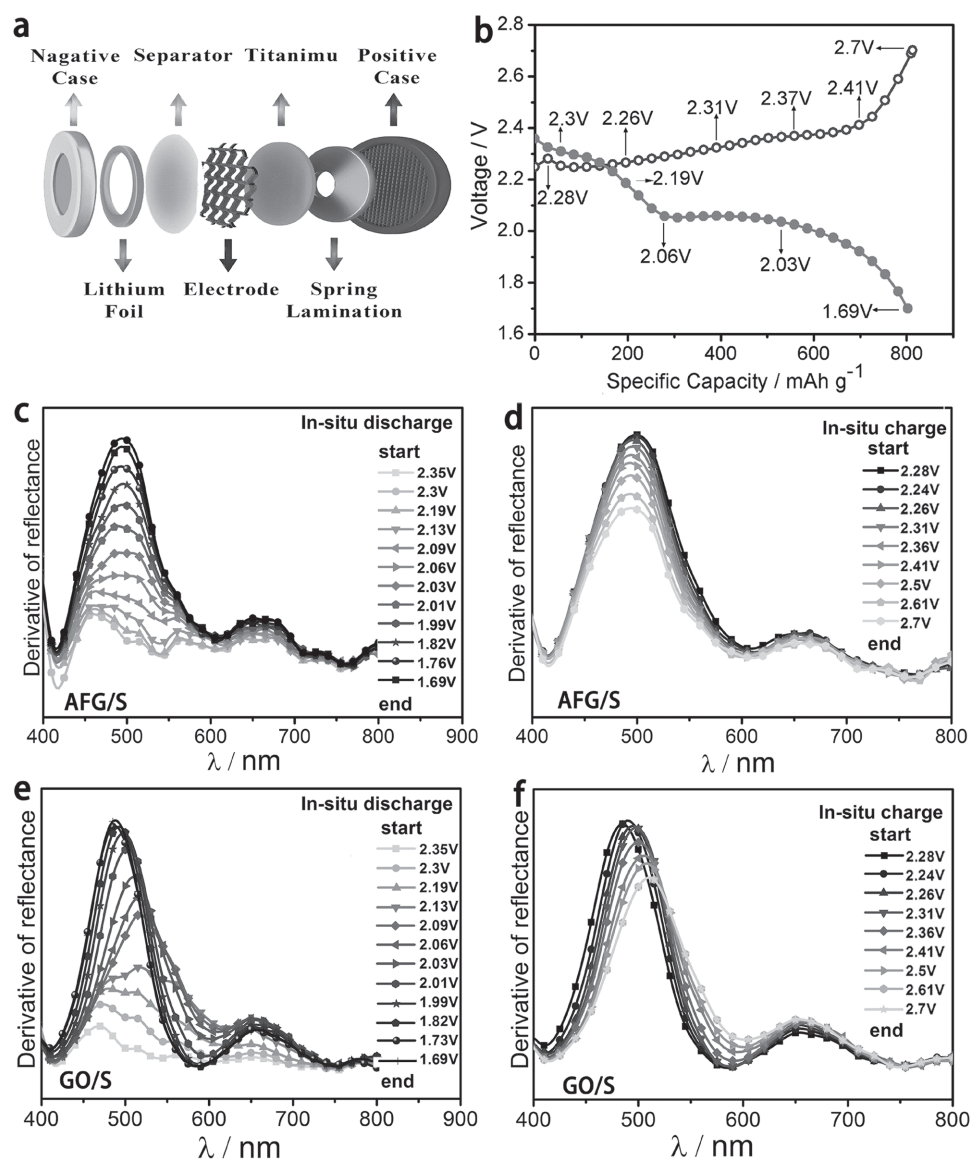

Figure 3. a,b) The cell structure and the selected discharge/charge states of Li–S battery for in situ UV/vis spectra test. c,d) The corresponding first-order derivatives of the UV/vis spectra presented for AFG/S during discharging, respectively. e,f) The corresponding first-order derivatives of the UV/vis spectra presented for GO/S during charging, respectively.

ADVANCED
SCIENCE NEWS
www.advancedsciencenews.com

NANO · MICRO
small
www.small-journal.com

curves toward shorter wavelengths, indicating the appearance of short-chain polysulfides. This is further demonstrated by the first-order derivatives of the UV/vis spectra. A significant change in the peak position can be observed. During charging, the UV/vis spectra gradually shift from short wavelengths to longer wavelengths when the cell is charged from 2.28 to 2.7 V, corresponding to an increase in the chain length of polysulfides. Similar to GO/S, the spectra for rGO/S also reveal the formation of different types of long-chain lithium polysulfide intermediates (Figure S11, Supporting Information). By contrast, the UV/vis spectra for AFG/S cathode show significant differences. Upon discharging, the spectra exhibit almost no change in the reflection toward the higher wavelengths. As only short-chain polysulfides are formed, all the spectra show strong absorbance toward short wavelengths, which is in accordance with the results observed from the derivative curves. As presented in Figure 3c, initially, the derivative curves display relatively weak peaks at higher wavelengths, probably due to the reaction between free sulfur and lithium. As the discharge proceeds, the maxima at $\lambda = 490$ nm appeared, which should be ascribed to the exclusive products of short-chain polysulfides. To further understand the interactions between Li^+ and AFG/S nanocomposites, quantitative investigation on the cleavage of S—S bonds is performed using a density functional theory exchange-correlation functional (DFT). As shown in **Figure 4**c, the calculations indicate the dissociation energy of -16.14 kcal mol^{-1} for the S_4—S_5 bond, which is the lowest compared with the cleavage of other

S—S bonds. The calculations demonstrate the highly favorable aspects of covalent attachment of S_8 onto the thiol-grafted graphene, with findings in agreement with in situ UV/vis spectra discussed above. The hypothetical illustration of the multistep discharging process is displayed in Figure 4. Initially, Li^+ is dynamically inserted into the crosslinked linear polysulfane, forming the long-chain lithium polysulfides, which are covalently attached onto graphene nanosheets. Further insertion reaction results in the S—S bond break of lithium polysulfides. Meanwhile, short-chain polysulfides are formed and deposited on the graphene backbone, which could effectively avoid the shuttling effect of long-chain polysulfides.

In summary, we proposed an effective strategy to crosslink the linear polysulfane onto graphene nanosheets to stabilize the performance of lithium–sulfur battery. DFT calculations demonstrate that the fracture of crosslinked sulfur chains in the present copolymer is prone to happen in the middle position (S_4—S_5 bond), with the lowest dissociation energy of -16.14 kcal mol^{-1}. Further cleavage produces short-chain polysulfides as the only product. Similarly, in situ UV/vis spectroscopy, coupled with the derivative curves, has also illustrated that only short-chain polysulfides are produced throughout the charging and discharging process, which is in stark contrast to GO/S composites. As a result, the synthesized copolymer enables us to achieve excellent capacity retention of 71.2% after 600 cycles, which conclude that AFG/S copolymers are very promising candidates for advanced Li–S batteries.
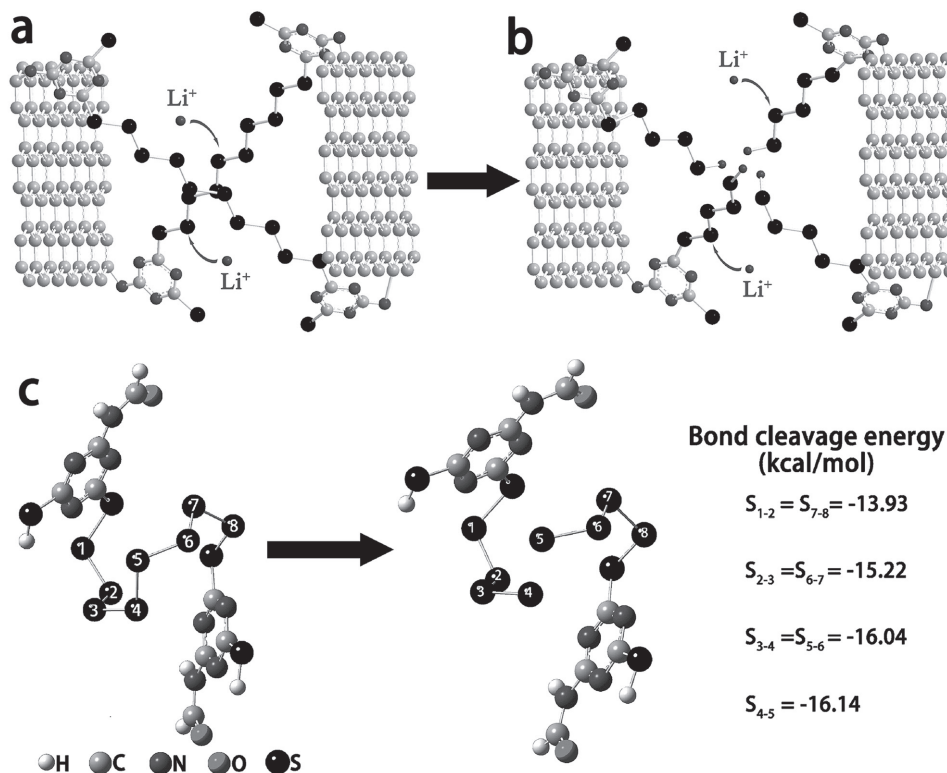

Figure 4. a,b) Schematic illustrations describing the electrochemical mechanism of AFG/S cathode. Further reaction with the covalently anchored lithium polysulfides results in the formation of short-chain polysulfides. c) DFT calculations showing the bond cleavage energy of S—S bonds, indicating the highly favorable aspects of covalent attachment of S_8 onto the thiol-grafted graphene.

[1] a) T. V. Choudhary, J. Malandra, J. Green, S. Parrott, B. Johnson, *Angew. Chem., Int. Ed.* **2006**, *45*, 3299; b) R. T. Yang, A. J. Hernandez-Maldonado, F. H. Yang, *Science* **2003**, *301*, 79; c) J. L. Lim, J. Pyun, K. Char, *Angew. Chem., Int. Ed.* **2015**, *54*, 3249.

[2] a) R. Xu, J. Lu, K. Amine, *Adv. Energy Mater.* **2015**, *5*, 1; b) D. W. Wang, Q. C. Zeng, G. M. Zhou, L. C. Yin, F. Li, H. M. Cheng, I. R. Gentle, G. Q. M. Lu, *J. Mater. Chem. A* **2013**, *1*, 9382.

[3] T. Rauchfuss, *Nat. Chem.* **2011**, *3*, 648.

[4] a) S. Y. Wei, L. Ma, K. E. Hendrickson, Z. Y. Tu, L. A. Archer, *J. Am. Chem. Soc.* **2015**, *137*, 12143; b) B. Oschmann, J. Park, C. Kim, K. Char, Y. E. Sung, R. Zentel, *Chem. Mater.* **2015**, *27*, 7011; c) S. F. Zhuo, Y. Huang, C. B. Liu, H. Wang, B. Zhang, *Chem. Commun.* **2014**, *50*, 11208; d) W. J. Chung, A. G. Simmonds, J. J. Griebel, E. T. Kim, H. S. Suh, I. B. Shim, R. S. Glass, D. A. Loy, P. Theato, Y. E. Sung, K. Char, J. Pyun, *Angew. Chem., Int. Ed.* **2011**, *50*, 11409.

[5] a) S. Urbonaite, T. Poux, P. Novák, *Adv. Energy Mater.* **2015**, *5*, 1; b) L. W. Ji, M. M. Rao, H. M. Zheng, L. Zhang, Y. C. Li, W. H. Duan, J. H. Guo, E. J. Cairns, Y. G. Zhang, *J. Am. Chem. Soc.* **2011**, *133*, 18522; c) Y. C. Qiu, W. F. Li, W. Zhao, G. Z. Li, Y. Hou, M. N. Liu, L. S. Zhou, F. M. Ye, H. F. Li, Z. H. Wei, S. H. Yang, W. H. Duan, Y. F. Ye, J. H. Guo, Y. G. Zhang, *Nano Lett.* **2014**, *14*, 4821; d) H. W. Chen, C. H. Wang, W. L. Dong, W. Lu, Z. L. Du, L. W. Chen, *Nano Lett.* **2015**, *15*, 798; e) J. Z. Chen, K. S. Han, W. A. Henderson, K. C. Lau, M. Vijayakumar, T. Dzwiniel, H. L. Pan, L. A. Curtiss, J. Xiao, K. T. Mueller, Y. Y. Shao, J. Liu, *Adv. Energy Mater.* **2016**, *6*, 1600160; f) H. J. Peng, Z. W. Zhang, J. Q. Huang, G. Zhang, J. Xie, W. T. Xu, J. L. Shi, X. Chen, X. B. Cheng, Q. Zhang, *Adv. Mater.* **2016**, *28*, 9551; g) X. Y. Tao, J. G. Wang, C. Liu, H. T. Wang, H. B. Yao,

G. Y. Zheng, Z. W. Seh, Q. X. Cai, W. Y. Li, G. M. Zhou, C. X. Zu, Y. Cui, *Nat. Commun.* **2016**, *7*, 11203.

[6] a) D. Bresser, S. Passerini, B. Scrosati, *Chem. Commun.* **2013**, *49*, 10545; b) J. Q. Zhou, T. Qian, N. Xu, M. F. Wang, X. Y. Ni, X. J. Liu, X. W. Shen, C. L. Yan, *Adv. Mater.* **2017**, *29*, 1701294.

[7] G. He, S. Evers, X. Liang, M. Cuisinier, A. Garsuch, L. F. Nazar, *ACS Nano* **2013**, *7*, 10920.

[8] a) Z. Y. Wang, Y. F. Dong, H. J. Li, Z. B. Zhao, H. B. Wu, C. Hao, S. H. Liu, J. S. Qiu, X. W. Lou, *Nat. Commun.* **2014**, *5*, 1; b) X. Y. Tao, J. G. Wang, Z. G. Ying, Q. X. Cai, G. Y. Zheng, Y. P. Gan, H. Huang, Y. Xia, C. Liang, W. K Zhang, Y Cui, *Nano Lett.* **2014**, *14*, 5288; c) Z. Yuan, H. J. Peng, T. Z. Hou, J. Q. Huang, C. M. Chen, D. W. Wang, X. B. Cheng, F. Wei, Q. Zhang, *Nano Lett.* **2016**, *16*, 519; d) J. Liu, T. Qian, M. F. Wang, X. J. Liu, N. Xu, Y. Z. You, C. L. Yan, *Nano Lett.* **2017**, *17*, 5064

[9] a) H. Hu, H. Y. Cheng, Z. F. Liu, G. J. Li, Q. C. Zhu, Y. Yu, *Nano Lett.* **2015**, *15*, 5116; b) C. F. Zhang, H. B. Wu, C. Z. Yuan, Z. P. Guo, X. W. Lou, *Angew. Chem.* **2012**, *124*, 9730; c) G. M. Zhou, L. C. Yin, D. W. Wang, L. Li, S. F. Pei, I. R. Gentle, F. Li, H. M. Cheng, *ACS Nano* **2013**, *7*, 5367; d) R. P. Fang, S. Y. Zhao, S. F Pei, X. T. Qian, P. X. Hou, H. M. Cheng, C. Liu, F. Li, *ACS Nano* **2016**, *10*, 8676; e) C. Tang, B. Q. Li, Q. Zhang, L. Zhu, H.F. Wang, J. L. Shi, F. Wei, *Adv. Funct. Mater.* **2016**, *26*, 577; f) H. B. Yao, G. Y. Zheng, P. C. Hsu, D. S. Kong, J. J. Cha, W. Y. Li, Z. W. Seh, M. T. McDowell1, K. Yan, Z. Liang, V. K. Narasimhan, Yi Cui, *Nat. Commun.* **2014**, *5*, 3943; g) Z. H. Sun, J. Q. Zhang, L. C. Yin, G. J. Hu, R. P. Fang, H. M. Cheng, F. Li, *Nat. Commun.* **2017**, *8*, 14627; h) F. Zhou, L. T. Song, L. L. Lu, H. B. Yao, S. H. Yu, *ChemNanoMat* **2016**, *2*, 937.

[10] a) H. B. Yao, G. Y. Zheng, P. C. Hsu, D. S. Kong, J. J. Cha, W. Y. Li, Z. W. Seh, M. T. McDowell, K. Yan, Z. Liang, V. K. Narasimhan, Y. Cui, *Nat. Commun.* **2014**, *5*, 3943; b) Z. H. Sun, J. Q. Zhang, L. C. Yin, G. J. Hu, R. P. Fang, H. M. Cheng, F. Li, *Nat. Commun.* **2017**, *8*, 14627; c) F. Zhou, L. T. Song, L. L. Lu, H. B. Yao, S. H. Yu, *ChemNanoMat* **2016**, *2*, 937.

[11] W. J. Chung, J. J. Griebel, E. T. Kim, H. Yoon, A. G. Simmonds, H. J. Ji, P. T. Dirlam, R. S. Glass, J. J. Wie, N. A. Nguyen, B. W. Guralnick, J. Park, A. Somogyi, P. Theato, M. E. Mackay, Y. E. Sung, K. Char, J. Pyun, *Nat. Chem.* **2013**, *5*, 518.

[12] S. N. Talapaneni, T. H. Hwang, S. H. Je, O. Buyukcakir, J. W. Choi, A. Coskun, *Angew. Chem., Int. Ed.* **2016**, *55*, 3106.

[13] a) H. Hu, Z. B. Zhao, W. B. Wan, Y. Gogotsi, J. S. Qiu, *Adv. Mater.* **2013**, *25*, 2219; b) J. J. Xie, Y. Zhang, Y. L. Han, C. L. Li, *ACS Nano* **2016**, *10*, 5304; c) W. B. Wan, L. L. Li, Z. B. Zhao, H. Hu, X. J. Hao, D. A. Winkler, L. C. Xi, T. C. Hughes, J. S. Qiu, *Adv. Funct. Mater.* **2014**, *24*, 4915.

[14] Z. S. Wu, A. Winter, L. Chen, Y. Sun, A. Turchanin, X. L. Feng, K. Müllen, *Adv. Mater.* **2012**, *24*, 5130.

[15] G. M. Zhou, Y. B. Zhao, A. Manthiram, *Adv. Energy Mater.* **2015**, *5*, 1402263.

[16] G. M. Zhou, E. Paek, G. S. Hwang, A. Manthiram, *Nat. Commun.* **2015**, *6*, 7760.

[17] Y. S. Su, Y. Z. Fu, T. Cochell, A. Manthiram, *Nat. Commun.* **2013**, *4*, 2985.

[18] H. Kim, J. Lee, H. Ahn, O. Kim, M. J. Park, *Nat. Commun.* **2015**, *6*, 7278.

[19] a) M. U. M. Patel, R. Dominko, *ChemSusChem* **2014**, *7*, 2167; b) M. U. M. Patel, R. Demir-Cakan, M. Morcrette, J. M. Tarascon, M. Gaberscek, R. Dominko, *ChemSusChem* **2013**, *6*, 1177; c) W. Chen, T. Qian, J. Xiong, N. Xu, X. J. Liu, J. Liu, J. Q. Zhou, X. W. Shen, T. Z. Yang, Y. Chen, C. L. Yan, *Adv. Mater.* **2017**, *29*, 1605160.